

High solubility pathway for the carbon dioxide free production of iron†

Stuart Licht* and Baohui Wang‡

Received 26th May 2010, Accepted 10th August 2010

DOI: 10.1039/c0cc01594f

We report a fundamental change in the understanding of iron oxide thermochemistry, opening a facile, new CO₂-free route to iron production. The resultant process can eliminate a major global source of greenhouse gas emission, producing the staple iron in molten media at high rate and low electrolysis energy.

Along with control of fire, the carbothermal reduction of iron is one of the founding technological pillars of civilization. Yet, it is also one of the major global sources of greenhouse gas release. In industry, iron is still produced by the greenhouse gas intensive reduction of iron oxide by carbon-coke, and a CO₂-free process to form this staple is needed. We report a significant change in the value of the free energy and solubility product (17 order of magnitude increase) of Fe₂O₃ at elevated temperatures leading to a carbon dioxide free process for the production of iron. This process is of significance as it can lead to elimination of one of the major global sources of greenhouse gas release. The earliest attempt at electrowinning iron from carbonate appears to have been in 1944 in the unsuccessful attempt to electrodeposit iron from a sodium carbonate, peroxide, metaborate mix at 450–500 °C, which deposited sodium and magnetite (iron oxide), rather than iron.^{1,2} Later attempts have focused on the electrodeposition of iron from molten mixed chloride/fluoride electrolytes.^{3,4} A brief overview of iron history is in the ESI.†

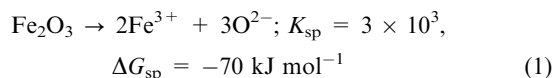
Here we show, a novel route to generate iron metal by the electrolysis of dissolved iron oxide salts in molten carbonate electrolytes, unexpected due to the reported insolubility of iron oxide in carbonates. This process will prevent the extensive release of carbon dioxide, which currently accompanies the formation of iron metal from iron ores. We demonstrate this CO₂-free process with the reduction of either Fe₂O₃, available as the common mineral hematite, or Fe₃O₄, available as the common mineral magnetite, to form iron metal at high electrolysis current density and low electrolysis energy. The low electrolysis energy can be driven by conventional electrical sources, but is also consistent with a new STEP (Solar Thermal Electrochemical Photo) process for electrolysis without any evolution of carbon dioxide.^{5,6}

Ferric carbonate does not appear in nature due to the relative acidity of the aqueous Fe³⁺ cation (which forms ferric hydroxide and evolves CO₂). As recently as 1999, the solubility

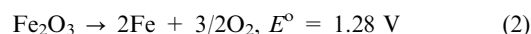
of ferric oxide, Fe₂O₃, in 650 °C molten carbonate was reported as very low, a 10^{−4.4} mole fraction ($K_{sp} = 4 \times 10^{-14}$; $\Delta G_{sp} = 240 \text{ kJ mol}^{-1}$) in lithium/potassium carbonate mixtures. Furthermore, the solubility was reported as an invariant of the fraction of Li₂CO₃ and K₂CO₃ in these lithium/potassium carbonate mixtures.⁷ These low solubility studies, of interest to the optimization of molten carbonate fuel cells, have likely discouraged research into the electrowinning of iron metal from ferric oxide in molten lithium carbonate.

We report that at higher temperature, molten lithium carbonate is an effective medium for the electrolytic deposition of iron metal. Unlike the current industry process, iron is formed from molten lithium carbonate without the release of greenhouse gas. The thermodynamic potentials for the reduction of iron oxides to iron will be shown to be endothermic; this decrease, with increasing temperature, will result in considerable energy savings compared to lower temperature electrolysis, when solar thermal and solar PV energy is applied, as in the STEP process.^{5,6}

Ferric oxide (99.6%, JT Baker) heated alone remains a red powder. However, when heated in contact with solid Li₂CO₃ powder (Alfa, 99%), we observe it is highly soluble in molten Li₂CO₃. Li₂CO₃ (mp 723 °C) is transparent, and takes on a red colour with dissolution of the Fe₂O₃. A mixture of one part Fe₂O₃ to 5 parts (by mass) Li₂CO₃ contains some solid Fe₂O₃ at 750 °C, but is fully molten by 800 °C, for a mole fraction solubility of 0.085 (2 M), and in accord with:



This 17 order of magnitude increase in the Fe₂O₃ solubility constant sustains a significant concentration of iron in the molten salt, and provides a route for the facile electrolytic generation of iron metal. The cyclic voltammetry (CV) at 800 °C of this molten, 1 to 5 Fe₂O₃ to Li₂CO₃ electrolyte is presented in Fig. 1, and exhibits a clear reduction peak at −0.8 V, on platinum (dark orange curve); the peak is more pronounced at an iron electrode (light orange curve). At constant current, iron is clearly deposited. The cooled deposited product contains pure iron metal and trapped salt, and changes to rust colour with exposure to water (Fig. 1, photo top left). The net electrolysis is the redox reaction of ferric oxide to iron metal and oxygen:



The washed, electrolysis product weight is consistent with >90% complete conversion of the 6 electron per Fe₂O₃ coulombic reduction to iron, during 1 hour of electrolysis at either 200 or 20 mA cm^{−2} of iron deposition. The measured coulombic efficiency rises to a minimum of 97% on repetition,

Department of Chemistry, George Washington University, Ashburn, Virginia 20147, USA. E-mail: slicht@gwu.edu; Tel: +1 703 726 8215

† Electronic supplementary information (ESI) available: A brief overview of iron history, mechanism and calculated decrease of CO₂ emissions with new STEP electrolysis, description of solar thermal electrochemical photo energy conversion, and comparison of alkali carbonate electrolytes. See DOI: 10.1039/c0cc01594f

‡ Present address: Northeast Petroleum University, Daqing, P. R. China.

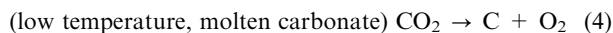
with care to prevent material loss during washing. The extracted deposited mass contains pure iron metal, and trapped salt, which is washed to remove the trapped salt by (1) grinding to a fine powder, (2) sonication in water for 30 minutes, (3) settling for 0.5 minute, then pouring off the colloidal suspension and liquid from the precipitate. Steps 2 and 3 are repeated several times with the precipitate, which is then observed to be reflective, grey and metallic. This is followed by further washing, sonicating and decanting the precipitate, respectively, in methanol, acetone and *n*-hexane (*n*-hexane wash is not necessary, but demonstrates that carbon is not present), followed by 10 minutes of vacuum drying and weighing. The product, dendritic iron crystals, is stored in acetone, and responds uniformly to an external magnetic field.

The two principle ores of iron are hematite (Fe_2O_3) and the mixed valence $\text{Fe}^{2+/3+}$ magnetite (Fe_3O_4). We observe that Fe_3O_4 is also highly soluble in molten Li_2CO_3 , and may be reduced to iron with the net electrolysis reaction:



Fe_3O_4 is a black powder (Pflatz & Bauer 99.9%), which forms a black liquid on dissolution in a molten Li_2CO_3 . As seen in Fig. 1 photo (right side), and as with the Fe_2O_3 case, the extracted cooled electrode, following extended electrolysis and iron formation, contains trapped electrolyte. Following 1 hour of electrolysis at either 200 or 20 mA cm^{-2} of iron deposition, and the washing procedure described for the Fe_2O_3 (without the hexane step), the product weight is consistent with a complete 8 electron per Fe_3O_4 coulombic reduction to iron.

The lower portion of Fig. 1 compares the cyclic voltammetry of Fe_2O_3 and Fe_3O_4 in molten Li_2CO_3 at 800 °C. Unlike the single peak evident for Fe_2O_3 , two reduction peaks appear for Fe_3O_4 . Following the initial cathodic sweep (indicated by the left arrow), the CV at Pt exhibits two reduction peaks (black curve), which are more pronounced at an iron electrode (grey curve). The Fe_3O_4 peaks observed at -0.6 V and -0.76 V appear to be consistent with the respective reductions of Fe^{2+} and Fe^{3+} . In either Fe_2O_3 or Fe_3O_4 , molten Li_2CO_3 electrolytes, the reduction occurs at a potential before we observe any reduction of the electrolyte, and at constant current, iron is deposited. In iron-free Li_2CO_3 , electrolysis of CO_2 to C or CO has been detailed.⁶



In Fig. 2, our calculated thermodynamic electrolysis potentials for the conversion of Fe_2O_3 or Fe_3O_4 to iron and O_2 , eqn (2) and (3), are plotted with the circle symbols. The processes are each endothermic; the required electrolysis potential decreases with increasing temperature. The thermodynamic electrolysis potentials for Fe_2O_3 are $\sim 0.06 \text{ V}$ lower than for Fe_3O_4 , and in the temperature domain of molten Li_2CO_3 , each is considerably below their respective rest potentials at 25 °C of 1.28 and 1.32 V. As seen in the figure, the experimental electrolysis potentials at a constant 0.050 A are similar for Fe_2O_3 and Fe_3O_4 at 800 °C, but at $T > 800 \text{ }^\circ\text{C}$ are lower for the Fe_2O_3 containing electrolyte. At high

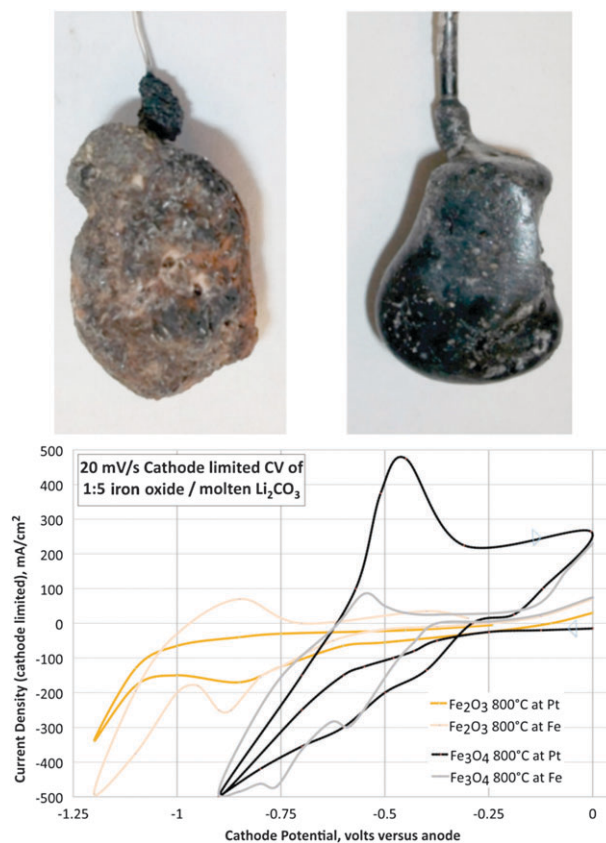
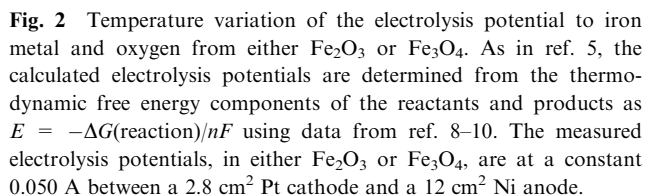


Fig. 1 Top: photographs of electrolysis product from in 800 °C molten Li_2CO_3 : (left side) following 0.5 A electrolysis in Fe_2O_3 for 2 hours on coiled 2.8 cm^2 platinum wire ($d = 0.5 \text{ mm}$). The 4.8 g mass shown on the electrode contains 0.8 g iron metal (following grinding and cleaning); (right side) following 0.5 A electrolysis in Fe_3O_4 for 1 hour on coiled 7.0 cm^2 iron wire ($d = 1.5 \text{ mm}$). Each case uses 16 g of the iron oxide in 80 g Li_2CO_3 in a 75 ml alumina crucible. Bottom: cathode restricted cyclic voltammetry in 800 °C molten Li_2CO_3 , containing 1 : 5 by weight of either Fe_2O_3 or Fe_3O_4 . The measured potential is dominated by the cathode overpotential through the use of a 60-fold excess of anode surface area.

temperature it is seen that the measured electrolysis potential can fall below the thermodynamic potential. The latter is calculated at unit activity, and the former may reflect a Nernst, non-unit activity variation of the potential. The sharp drop in electrolysis potential occurring at $T > 850 \text{ }^\circ\text{C}$ parallels our previous observation in iron-free molten Li_2CO_3 in which the main electrolysis product switches from solid C to CO at these temperatures.⁶

The advantages of a Li_2CO_3 , compared to Na_2CO_3 or K_2CO_3 electrolyte, are described in the ESI.† The measured full cell electrolysis potential, E , of Fe_2O_3 or Fe_3O_4 in Li_2CO_3 for a range of constant current densities, J , is presented in Table 1. J is determined by the cathode surface area. The subscript SA in J or E denotes a small (4-fold excess), and LA a large (60-fold excess) surface area of anode. The measured potentials are similar with smooth Pt or iron cathodes, and with anodes of smooth Pt or Ni (nickel oxide, prepared as McMaster 200 pure Ni sheet). E is stable during continuous electrolysis at this range of J . Comparing large and small relative anodes in Table 1, it is evident that anode (O_2 , rather



$J_{\text{LA}}/\text{mA cm}^{-2}$	3	20	200	500
$E(\text{Fe}_2\text{O}_3)_{\text{LA}}$	0.85 V	1.18 V	1.40 V	1.70 V
$E(\text{Fe}_3\text{O}_4)_{\text{LA}}$			0.60 V	0.90 V
$J_{\text{SA}}/\text{mA cm}^{-2}$	7	18	70	200
$E(\text{Fe}_2\text{O}_3)_{\text{SA}}$	1.15 V	1.25 V	1.57 V	1.70 V
$E(\text{Fe}_3\text{O}_4)_{\text{SA}}$		1.27 V		1.70 V

The low voltage iron carbonate electrolysis presented in this study can be driven by conventional or renewable electricity, respectively, with diminished or no CO₂ emission, as delineated in the ESI.† The decrease in electrolysis potential with increasing temperature presents a low energy electrolysis opportunity for the STEP process. In this process solar thermal provides heat to decrease the electrolysis potential, and solar visible generates electronic charge to drive the electrolysis. The synergistic use of both visible and infrared sunlight provides high solar energy conversion efficiencies (STEP energy diagram is in the ESI†).^{5,6} Eqn (2) and (3) provide, in molten carbonate electrolytes, low energy routes for the carbon dioxide free formation of iron metal from iron ores. We use a 37% solar energy conversion efficient concentrator photovoltaic (CPV) as a convenient power source to drive the low electrolysis energy iron deposition without CO₂ formation as schematically represented in Fig. 3. Details of the CPV and STEP experimental configurations in the Li₂CO₃ electrolyte for CO₂ reduction are given in ref. 6.

The diagram illustrates a solar-driven molten carbonate electrolysis cell (MCEC) system for Fe₂O₃ production. The system consists of a solar CPV power source, a molten Li₂CO₃ electrolyte, and two MCEC units.

Solar Energy Conversion: Sunlight is converted by solar-PV cells (Q_{solar-PV}) and solar-IR cells (Q_{solar-IR}). The solar-IR cells are heated by Fe₂O₃ or Fe₃O₄.

Molten Carbonate Electrolysis Cell (MCEC): The MCEC units use electricity to electrolyze molten Li₂CO₃, producing iron and O₂. The O₂ is used to produce Fe₂O₃ in the solar-IR cells.

Ga(In)As Multi-junction Solar Cell Structure: The diagram shows a detailed cross-section of a Ga(In)As multi-junction solar cell. The layers from top to bottom are: contact, n-Ga(In)As, AR (anti-reflection), n-Ga(In)As emitter, p-Ga(In)As base, p-AlGaInP BSF, p-n junction, tunnel junction, n-Ga(In)As emitter, p-Ga(In)As base, p-Ga(In)As BSF, p-n junction, tunnel junction, n-Ga(In)As buffer, n-Ga(In)As emitter, p-Ga(In)As substrate, and contact.

increasing temperature, provides a new route for iron production. Iron is formed without an extensive release of CO_2 in a process compatible with the predominant naturally occurring iron oxide ores, hematite, Fe_2O_3 , and magnetite, Fe_3O_4 . Iron, a basic commodity, currently accounts for the release of one quarter of worldwide CO_2 emissions by industries. The endothermic nature of the new synthesis route provides an effective vehicle for the solar efficient, CO_2 free, production of iron as a STEP process.

- 1 L. Andrieux and G. Weiss, *Comptes Rendus*, 1944, **217**, 615.
- 2 G. M. Haarberg, E. Kvalheim, S. Rolseth, T. Murakami, S. Pietrzyk and S. Wang, *ECS Trans.*, 2007, **3**, 341.
- 3 S. Wang, G. M. Haarberg and E. Kvalheim, *J. Iron Steel Res. Int.*, 2008, **15**, 48.
- 4 G. M. Li, D. H. Wang and Z. Chen, *J. Mater. Sci. Technol. (Shenyang, People's Repub. China)*, 2009, **25**, 767.
- 5 S. Licht, *J. Phys. Chem. C*, 2009, **113**, 16283.
- 6 S. Licht, B. Wang, S. Ghosh, H. Ayub, D. Jinag and J. Ganley, *J. Phys. Chem. Lett.*, 2010, **1**, 2363, online at: <http://pubs.acs.org/doi/abs/10.1021/jz100829s>.
- 7 L. Qinfeng, F. Borum, I. Petrushina and N. J. Bjerrum, *J. Electrochem. Soc.*, 1999, **146**, 2449.
- 8 M. W. Chase, Jr., NIST-JANAF Thermochemical Tables, 4th Edition, *J. Phys. Chem. Ref. Data*, 1998, **35**, 1.
- 9 J. D. Cox, D. Wagma and V. Medvedev, *CODATA Key Values for Thermodynamics*, Hemisphere Pub. Corp., NY, 1984.
- 10 Data from ref. 8 and 9 interactively available at: <http://webbook.nist.gov/chemistry/form-ser.html>.